Planck-LFI 44 GHz Back End Module

BEATRIZ AJA

JUAN PABLO PASCUAL

LUISA DE LA FUENTE

MARCO DETRATTI

EDUARDO ARTAL

ANGEL MEDIAVILLA
Universidad de Cantabria
Spain

PEDRO DE PACO
Universitat Autonoma de Barcelona
Spain

LLUIS PRADELL I CARA
Universitat Politecnica de Catalunya
Spain

This work describes the principle of operation, assembly and performance of one branch of the 44 GHz back end module (BEM) for the Planck low frequency instrument (LFI). This subsystem constitutes a fully representative branch of the qualification-model version (QM). It includes waveguide to microstrip transition, GaAs pseudomorphic high electron mobility transistor (PHEMT) low noise amplifiers (LNA), bandpass filter, square-law detector and dc amplifier. The fundamentals of the design of the RF part are described and all of the components have been tested individually before integration. Using single tone and wideband noise stimuli, the output voltage has been measured for several input powers, in order to obtain the sensitivity factor of the complete BEM. The effective bandwidth and the equivalent noise temperature have been calculated from the measurements, taking into account the frequency dependence on the noise source and the BEM. Finally the low frequency output power spectrum has been obtained and a maximum $1/f$ knee frequency around 200 Hz has been measured with a 3 dB output signal video bandwidth above 50 KHz.

Manuscript received May 12, 2004; revised December 21, 2004; released for publication April 11, 2005.

IEEE Log No. T-AES/41/4/860664.

Refereeing of this contribution was handled by M. Ruggieri.

This work was supported by the Plan Nacional de I+D+I, Programa Nacional de Espacio, ESP2002-04141-C03-01/02/03.

Authors' addresses: B. Aja, J. P. Pascual, L. de la Fuente, M. Detratti, E. Artal, and A. Mediavilla, Departamento de Ingenieria de Comunicaciones, ETSI Telecomunicacion, Universidad de Cantabria, Av. Los Castros, 39005 Santander, Spain, E-mail: (beatriz@dicom.unican.es); P. de Paco, Departamento de Telecomunicacion e Ingenieria de Sistemas, Universitat Autonoma de Barcelona (UAB-ETSE), Campus Bellaterra UAB, Edificio Q, 08193 Cerdanyola, Spain; L. Pradell i Cara, Departamento de Teoria del Senyal i Comunicacions, ETSE Telecomunicacio, Universitat Politecnica de Catalunya, Campus Nord, Modul D3, Calle Jordi Girona, 1, 08034 Barcelona, Spain.

I. INTRODUCTION

The Planck satellite is a mission of the European Space Agency, developed to measure extremely small temperature fluctuations of the cosmic microwave background (CMB) radiation over the sky. The low frequency instrument (LFI) receiver is a form of differential radiometer. It will have enough sensitivity to measure CMB anisotropies in the 30–70 GHz frequency range and it will be split into 3 channels centered at 30, 44, and 70 GHz each one with a 20 percent bandwidth [1–3].

The 30 and 44 GHz radiometers have been developed by Jodrell Bank Observatory in The United Kingdom and by the University of Cantabria and The Technical University of Catalonia in Spain [4]. The 70 GHz radiometers have been developed at Millilab in Finland [5]. The qualification models (QMs) at all frequencies have been developed and the flight models are under manufacture.

The radiometers collect the signal from the sky, which is amplified by low noise amplifiers (LNAs), and finally, filtered and detected. The 30 and 44 GHz radiometers are based on a front end module (FEM) with InP high electron mobility transistor (HEMT) amplifiers cooled to 20 K and a back end module (BEM) with GaAs HEMT amplifiers at room temperature (300 K), connected via a 1 m long waveguide. The FEM contains the most sensitive part of the receiver, where pseudocorrelation is implemented. It operates at 20 K to reduce the system noise and to improve sensitivity. This temperature is provided by a closed-cycle hydrogen sorption cryo-cooler [6], which will be capable of providing 1.2 W of cooling power at 20 K. This stringent requirement on low power consumption caused the decision to split the radiometer into a cold FEM and a warm BEM at 300 K. The gain specification in the FEM is 30 dB in order to provide enough gain to avoid a noise contribution to the system from the BEM. The LNAs in the FEM are comprised of InP HEMT due to their low power consumption and very good noise performance. The back end units at 30 and 44 GHz were developed in Spain with the cooperation of the University of Cantabria, Technical University of Catalonia and Mier Comunicaciones S.A.

A block diagram of the Planck radiometer is shown in Fig. 1. In fact each FEM and BEM assembly constitutes two complete and separate radiometers, due to the particular mechanical configuration of Planck-LFI. The sky signal and the signal from a stable reference load at about 4 K are coupled to cryogenic low-noise HEMT amplifiers via a 180° hybrid. One of the two signals then runs through a switch that applies a phase shift which oscillates between 0 and 180° at a frequency rate of 4096 Hz. A second phase switch is present for symmetry on the second radiometer leg but it does not introduce any

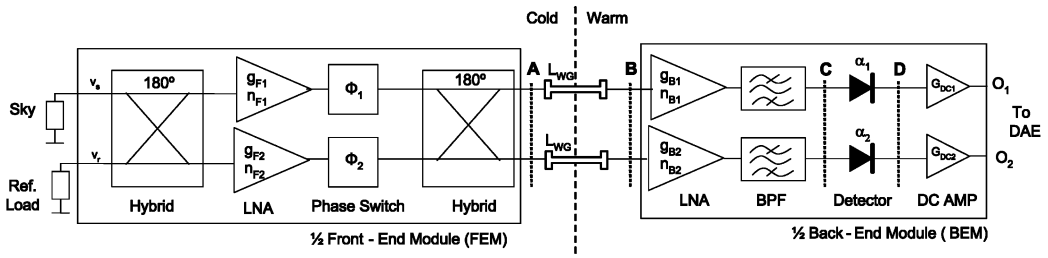

Fig. 1. Block diagram of Planck radiometer.

phase shift in the propagating signal. The signals are then recombined by a second 180° hybrid, producing an output which is a sequence of signals alternating at twice the phase switch frequency [7]. The output detected voltages at each of the two branches (O_1 and O_2) in the radiometer can be expressed as (1) and (2), respectively

$$V_{d1} = G_{DC1}\cdot\alpha_1\cdot\left|g_{B1}\cdot\left[\frac{1}{\sqrt{2}}\left(\left(\frac{v_s+v_r}{\sqrt{2}}+n_{F1}\right)\cdot g_{F1}\cdot e^{j\Phi1}+\left(\frac{v_s-v_r}{\sqrt{2}}+n_{F2}\right)\cdot g_{F2}\cdot e^{j\Phi2}\right)+n_{B1}\right]\right|^2 \quad (1)$$

$$V_{d2} = G_{DC2}\cdot\alpha_2\cdot\left|g_{B2}\cdot\left[\frac{1}{\sqrt{2}}\left(\left(\frac{v_s+v_r}{\sqrt{2}}+n_{F1}\right)\cdot g_{F1}\cdot e^{j\Phi1}-\left(\frac{v_s-v_r}{\sqrt{2}}+n_{F2}\right)\cdot g_{F2}\cdot e^{j\Phi2}\right)+n_{B2}\right]\right|^2 \quad (2)$$

where v_s is the noise voltage at the sky horn, v_r is the noise voltage at the reference load, g_{F1} and g_{F2} are the voltage gains of the two amplifiers in the FEM, and their noise voltage contributions are n_{F1} and n_{F2}. Φ_1 and Φ_2 are the phase values introduced by the phase shifters. The voltage gains in the BEM amplifiers are g_{B1} and g_{B2}, and n_{B1} and n_{B2} are their noise voltage contributions. The detector is considered to have a perfect square-law performance with a constant of proportionality of α_1 and α_2. In order to simplify the equations, both amplifiers in the FEM are considered to have identical gain g_F and each amplifier in the BEM also has the same gain g_B. Therefore the product of voltage gain in the FEM by voltage gain in the BEM is denominated as g.

One phase switch is placed in each FEM branch. It connects the LNA outputs to the output hybrid and it introduces a phase shift of 180° in the signal in one state in relation to the other. Only one phase switch works, the other is introduced for symmetry, therefore the phase Φ_1 will always be 0°. Therefore, the output voltage detected at one branch is proportional to the noise voltage at the sky horn v_s, or to the noise voltage at the reference load, v_r according to (3) and (4), respectively.

Case a Φ_1 and Φ_2 equal to 0°

$$V_{d1}(\phi_2=0) = G_{DC1}\cdot\alpha_1\cdot\left|g\cdot\left(v_s+\frac{n_{F1}+n_{F2}}{\sqrt{2}}+\frac{n_{B1}}{g_F}\right)\right|^2\cdot \quad (3)$$

Case b Φ_1 equal to 0° and Φ_2 equal to 180°

$$V_{d1}(\phi_2=180) = G_{DC1}\cdot\alpha_1\cdot\left|g\cdot\left(v_r+\frac{n_{F1}+n_{F2}}{\sqrt{2}}+\frac{n_{B1}}{g_F}\right)\right|^2. \quad (4)$$

With the phase switch active, the output voltage will change between sky and reference load at the two outputs. The signal of interest will be obtained by postprocessing of the output voltage and the goal is to nullify the signal measuring differences between the sky and the reference load. Therefore, a gain modulation factor r which balances the output, is applied [7, 9]. Calculating the time average of the output power over the bandwidth the expression of the gain modulation factor is given by (5)

$$r = \frac{T_{\text{sky}}+T_n}{T_{\text{load}}+T_n} \quad (5)$$

where T_{sky} is the sky noise temperature, T_{load} is the reference load temperature and, T_n is the system noise temperature. The r-factor will be adjusted periodically, therefore stability of the system is required. The instabilities due to gain and noise fluctuations produce a $1/f$ noise spectrum. The postprocessing signal must have a knee frequency (f_{knee}) lower than the spin frequency of the satellite. Phase switching in the FEM of a few KHz avoids the effect of BEM fluctuations providing that the BEM f_{knee} is lower than the phase switching rate.

The estimated postdetection knee frequency due to BEM gain fluctuations [7], considering a perfectly balanced FEM, is given by (6)

$$f_{\text{Knee}} = BW_{\text{eff}}\cdot N_s\cdot A^2 \quad (6)$$

where BW_{eff} is the effective bandwidth [8], N_s is the number of stages in the amplifier, and A is the normalization constant for noise temperature

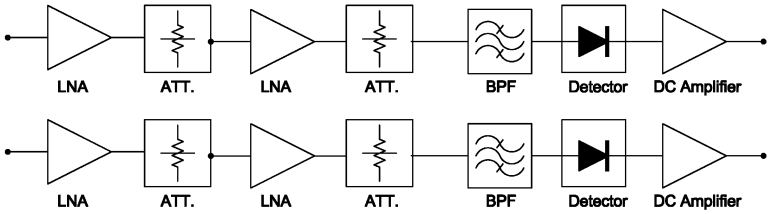

Fig. 2. Block diagram of 44 GHz BEM.

fluctuations. Using typical values for B, N_s, and A in (6) and considering only the RF amplifiers, the knee frequency expected from the BEM is only a few Hz. When fluctuations in the detector sensitivity are also considered, higher values are expected but always much lower than the phase switch frequency rate of about 4 KHz.

A. Power Budget

It is necessary to estimate the input power levels at the different stages of the BEM, in particular at the detector. For the power budget, one phase switch state is taken into account. The approximate power at the BEM input can be calculated according to (7)

$$P = \frac{kTBG_F}{L_{\mathrm{WG}}} \tag{7}$$

where k is Boltzmann's constant, B is the noise bandwidth, G_F is the FEM gain, L_{WG} are the losses of the waveguide connecting the FEM and the BEM, and $T = T_{\mathrm{FEM}} + T_i$, with T_{FEM} = FEM noise temperature, and T_i =input temperature (sky temperature ≈ 2.7 K or reference load ≈ 4 K). This input temperature will be fixed at 20 K for calibration, but it will oscillate between 2.7 K and 4 K in normal operation.

For the 44 GHz radiometer, the following parameters are specified:

$$BW_{\mathrm{eff}} = 8.8\ \mathrm{GHz}, \qquad G_F = 30\ \mathrm{dB}$$
$$L_{\mathrm{WG}} = 2\ \mathrm{dB}, \qquad T_{\mathrm{FEM}} = 10.4\ \mathrm{K}.$$

For an ideal system the noise bandwidth is equal to the effective bandwidth and using (7), the approximate BEM input power will be -60 dBm or -56 dBm, depending on whether the radiometer is working in normal operation or in calibration, respectively. The BEM gain is specified to be 30 dB with an equivalent noise temperature of 550 K, in order to ensure that the detector diode is working in its linear region with an estimated input power of about -30 dBm, this value being similar to others found in the literature [10]. A 20% effective bandwidth is necessary, which makes it difficult to fulfill the noise figure goal over the whole bandwidth. For the 44 GHz BEM, the RF circuits have been tested individually and then, the BEM representative branch has been measured. These results are shown in Sections II and IV, respectively.

II. CIRCUIT DESIGNS AND PERFORMANCE

Fig. 2 shows a block diagram of the 44 GHz BEM. A WR-22 waveguide-to-microstrip transition was designed using a ridge waveguide [11] and it is the first functional element of the BEM. It is a four-section stepped ridge waveguide-to-microstrip line transition which provides a broadband performance. This transition has been chosen for its broad bandwidth, low insertion loss, and repeatable performance.

A. Low Noise Amplifiers

The LNA is composed of two monolithic microwave integrated circuits (MMICs) to provide both enough gain and a signal in the square-law region of the diode detector. Since no suitable MMICs were commercially available, the LNAs were a custom design with GaAs PHEMT transistors. The technology chosen was OMMIC ED02AH process with an f_T of 60 GHz. The active pseudomorphic GaInAs layer is grown by hetero-epitaxy and it allows depletion or normally-on (N-ON) and enhancement or normally-off (N-OFF) PHEMT with a gate length of 0.2 μm [12]. The enhancement mode is similar in geometry to the depletion mode, but in electrical operation it is normally off and it does not conduct with zero gate voltage. The N-OFF mode has lower power consumption, nevertheless its gate voltage range is narrower than the N-ON mode, which provides a higher sensitivity to pinch-off voltage.

As for the disposition of LNAs, the N-ON LNA preceding the N-OFF was found to be the optimum of all those possible in terms of in-out matching, noise performance, and dc power consumption. Some of the main requirements of the LNAs are to provide low noise and low power consumption with sufficient gain. Using as the first amplifier an LNA based on N-ON PHEMT transistors, a good noise performance was obtained with a medium power consumption of 90 mW. The second LNA with N-OFF PHEMT transistors was added to increase the gain with a very low impact on the noise figure and a very low power consumption of 32 mW.

The two amplifiers have been designed using the same design method. A schematic of the Q-band four-stage MMIC LNAs is shown in Fig. 3. The first two stages use inductive source feedback to achieve a low noise performance [13] with good return loss.

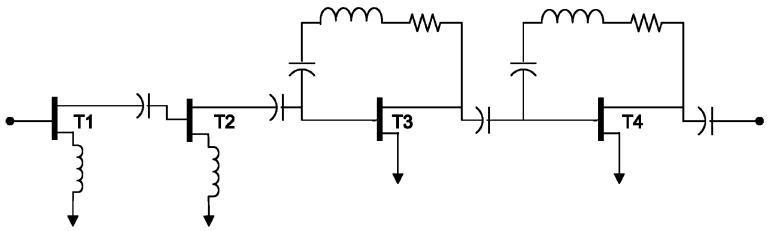

Fig. 3. Schematic of LNA.

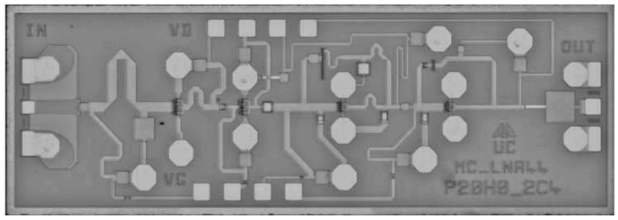

Fig. 4. N-ON LNA.

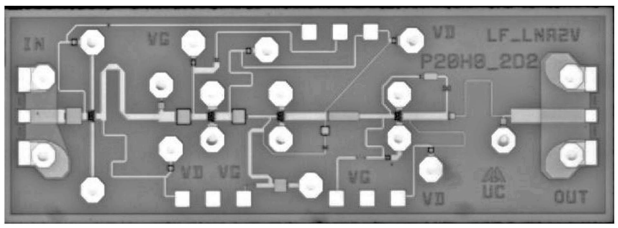

Fig. 5. N-OFF LNA.

Source inductors with different values have been employed for each stage in order to obtain a low noise figure with good input return loss and a reasonable gain, since in this way the last stages will have a small impact on the total noise figure. In the first stage minimum noise figure and conjugate matching are obtained by using a source inductor, but there is a trade-off with the achievable gain. Therefore the second stage was designed with a similar topology to the first one in order to obtain a slightly higher gain with low noise. Parallel feedback [14, 15] has been used in the last two stages to obtain flat gain over the operating bandwidth. This feedback has the advantage of increasing the stability factor, improving input, and output return losses.

Fig. 4 and Fig. 5 show the photographs of the LNAs. The chip size is 3×1 mm^2 each. Both circuits were measured on wafer using a coplanar probe station. In Fig. 6 and Fig. 7 noise figures and associated gain for the depletion and enhancement transistor LNAs are plotted. These amplifiers show an outstanding performance in gain and noise with a 20 percent bandwidth [16–18].

B. Bandpass Filter

A bandpass filter was used to define an effective bandwidth of 20% and to reject undesired signals outside the band of interest. Low bandpass losses, more than 10 dB out of band losses, and small size were considered the main objectives to fulfill. A microstrip coupled line topology was chosen because it inherently provides bandpass characteristics. A three-resonator filter has been designed using the design method from the classic prototype filter tables provided by [19] and a design methodology has been developed to achieve predictable frequency response in microstrip filters using commercial CAD software. After a careful evaluation of the validity of the CAD models, comparing simulated and accurately measured results, the design is restricted to microstrip elements than can be well characterized [20]. The selection of the substrate becomes critical due to the gaps and widths of microstrip lines because it sets the line-etching precision required and the minimum losses achievable. The filter has been fabricated on a Duroid 6002 ($\varepsilon_r = 2.94$) substrate with 0.254 mm thickness. Fig. 8 shows a photograph of the filter and Fig. 9 its response when it has been measured with coplanar to microstrip transitions using a coplanar probe station.

C. Diode Detector

After the signal is amplified and filtered, a square-law detector is used to convert the signal from the sky, or reference load, to dc voltage. The diode detector is based on a low barrier Schottky diode HSCH9161. A large and a small signal diode model have been developed to optimize the design. The matching network design requires additional lossy components to meet the system requirements. It uses a 100 Ω thick-film resistor. The resistor's nonideal behavior at millimeter frequency band had to be included in the simulations of the matching network. A radial stub is used to provide RF ground for the diode. The virtual ground was also used to extract the dc output voltage and a dc-return was provided by the 100 Ω resistor ground connection. A 100 KΩ load resistor was used as a video load impedance to extract the detected voltage. Input and output microstrip networks have been manufactured on Alumina substrate with a substrate thickness of 0.254 mm, permittivity $\varepsilon_r = 9.9$, conductor thickness $t = 3.5$ μm. This detector has been characterized individually with coplanar-to-microstrip transitions

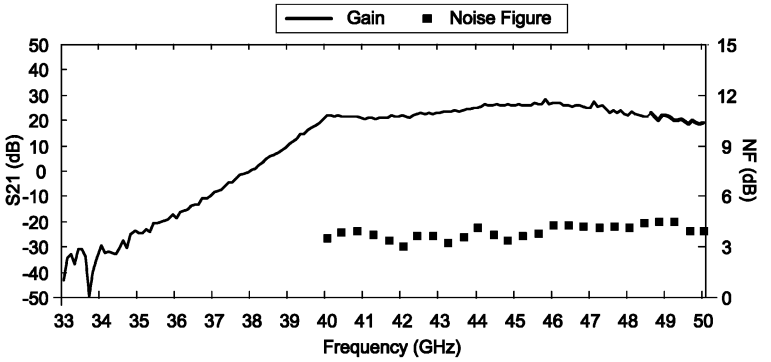

Fig. 6. N-ON LNA on-wafer performance.

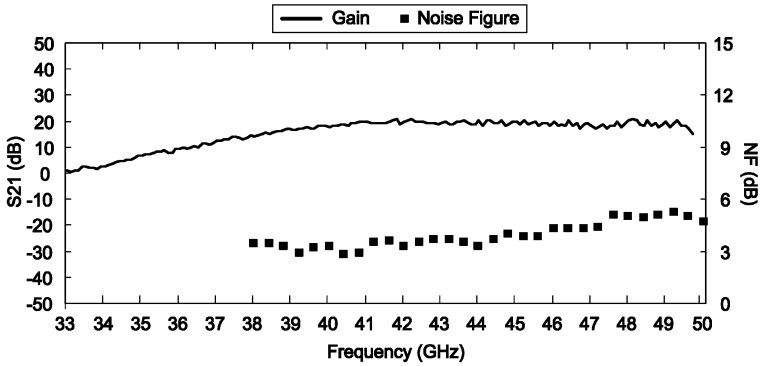

Fig. 7. N-OFF LNA on-wafer performance.

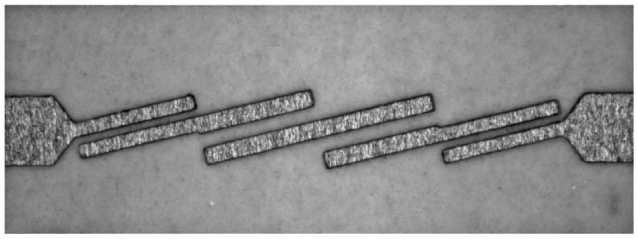

Fig. 8. Bandpass filter photograph.

using a coplanar probe station. Fig. 10 shows a photograph of the detector and Fig. 11 depicts its measured input return losses using a Vectorial network analyzer (HP8510C). Output detected voltage versus frequency is depicted in Fig. 12 (left). The detector sensitivity curve at 44 GHz has been included in the same figure (right), showing linear performance around −30 dBm of input power, this value being the expected input power to the detector.

D. Microstrip Attenuators

Two microstrip attenuators at the Q-band have been designed in order to obtain flat attenuation and good input and output matching. The aim of these attenuators was to get better matching between subsystems and reduce the ripple in band in order to provide better effective bandwidth.

The effective bandwidth [8] which is defined by (8), depends on the transducer power gain $G(f)$

$$BW_{\text{eff}} = \frac{\left[\int G(f)df\right]^2}{\int G^2(f)df}. \tag{8}$$

Transducer power gain of cascade networks depends on their matching in the plane of connection and on their individual transfer gain. The transfer gain of two connected networks, denominated A and B is given by (9)

$$G_T = |S_{21}|_A^2 \cdot |S_{21}|_B^2 \cdot \frac{1}{|1-\Gamma_1 \cdot \Gamma_2|^2} \tag{9}$$

where Γ_1 and Γ_2 are the reflection coefficients of the networks A and B, respectively, in their plane of connection. Therefore the effective bandwidth can be reduced by mismatching along the operating bandwidth.

The LNAs matching was not good enough, and so in order to minimize this effect on the effective bandwidth, attenuators were included between subsystems. Transducer power gain depends only on the forward transmission of each part.

The substrate used to design them was the same as for the detector. Resistors in the design are integrated thin film resistors in a NiCr layer with a resistivity of 20 Ohm/sq. Both designs have coplanar-to-microstrip transitions in order to allow their measurement with a coplanar probe station before their assembly. The final design of both attenuators with their

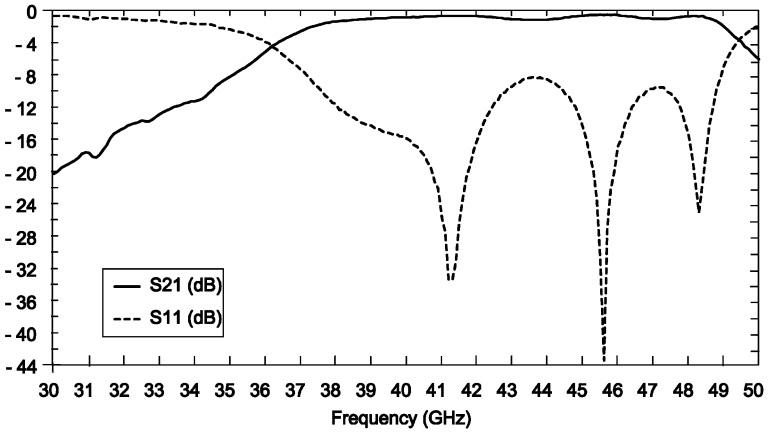

Fig. 9. Bandpass filter performance.

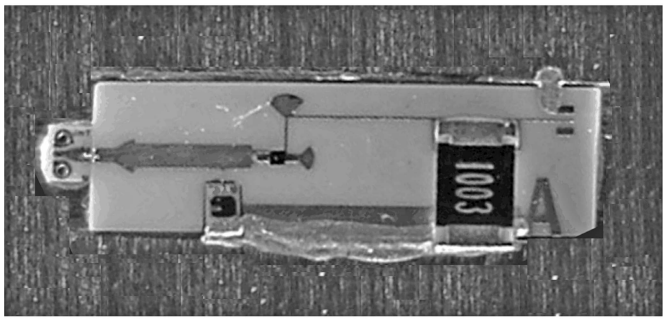

Fig. 10. Photograph of diode detector. From the left matching network including 100 Ohm resistor, diode connected to radial stub and 100 Kohm at the output.

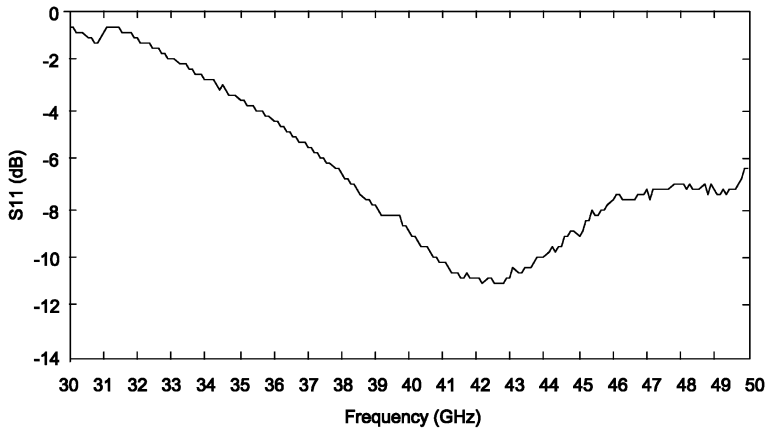

Fig. 11. Tested input matching of detector.

coplanar-to-microstrip transitions has been simulated using the electromagnetic quasi-3D simulator MOMENTUM. Fig. 13 and Fig. 14 show a picture of each attenuator. They have the same attenuation performance and the only difference between them is their length, one is 5 mm and the other is 10 mm. Both attenuators were characterized from 20 to 50 GHz using a coplanar probe station and a Vectorial Network Analyzer. Fig. 15 shows measured S-parameters of one attenuator. Both attenuators have similar performance with an attenuation of 4.7 dB in the operating bandwidth (39.6–48.4 GHz), and input and output matching better than 15 dB.

E. DC Amplifier

In order to make the detected signal suitable for the data acquisition electronic module, a low noise dc-amplifier has been designed. A schematic of the dc-amplifier is shown in Fig. 16. The first stage has an OP27 precision operational amplifier that combines low offset and drift characteristics with low noise, making it ideal for precision instrumentation

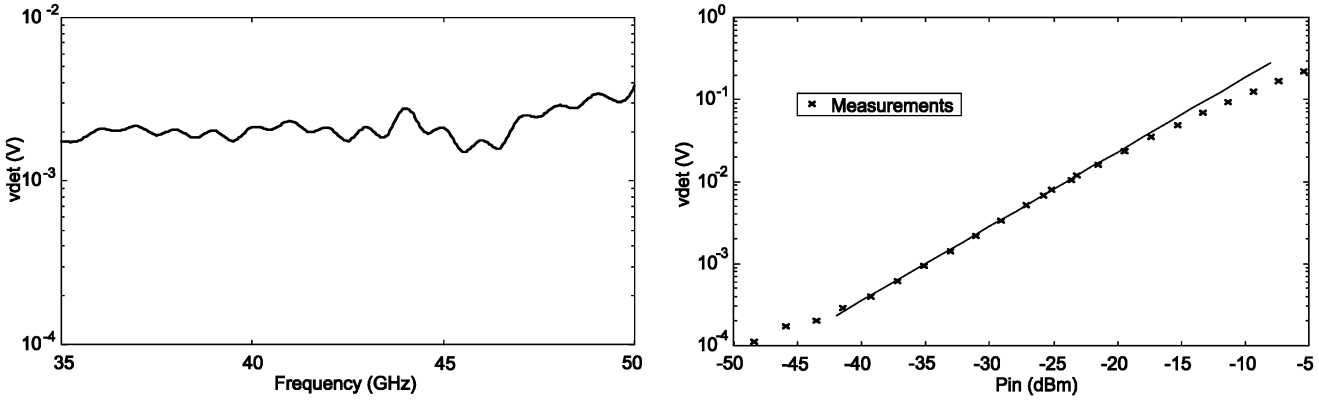

Fig. 12. Detected voltage frequency response with stimulus level of −30 dBm (left) and detector sensitivity at 44 GHz (right).

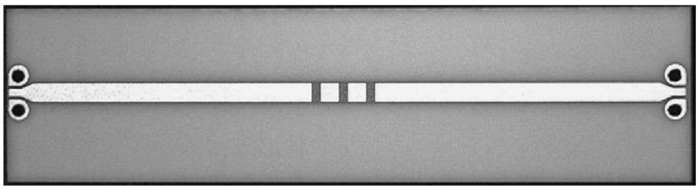

Fig. 13. First microstrip attenuator, length 10 mm.

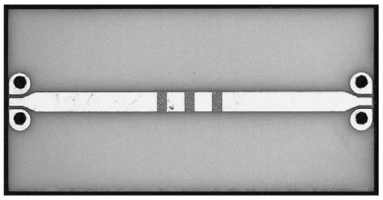

Fig. 14. Second microstrip attenuator, length 5 mm.

applications and accurate amplification of a low-level signal. A second balanced stage, implemented with an OP200, provides a balanced and bipolar output. DC amplifier total power consumption with a high impedance load is 37 mW approximately.

Since the phase switch frequency rate is 4096 Hz the output signal has to provide a video bandwidth of at least 50 KHz, which means that the output signal contains more than ten harmonics in order not to degrade the information. The OP27 operational amplifier gain bandwidth product has been taken into account, and the maximum achievable balanced gain without losing output bandwidth was 100. A voltage gain of 50 is due to the OP27 and factor 2 due to unbalanced-to-balanced conversion of the OP200 with unit individual gain. Another constraint of this dc amplifier is to provide an output voltage in a window between 0.2 V and 0.8 V, where the data acquisition electronics (DAE) works properly. The designed dc amplifier has an overall balanced voltage gain of 72, therefore the output dc voltage is inside the window and to achieve the output bandwidth requirement. The unbalanced frequency response of the LNA was tested using a vector signal analyzer and it is depicted in Fig. 17. The dc amplifier showed a video bandwidth of 65 KHz, and an unbalanced voltage gain of 31 dB.

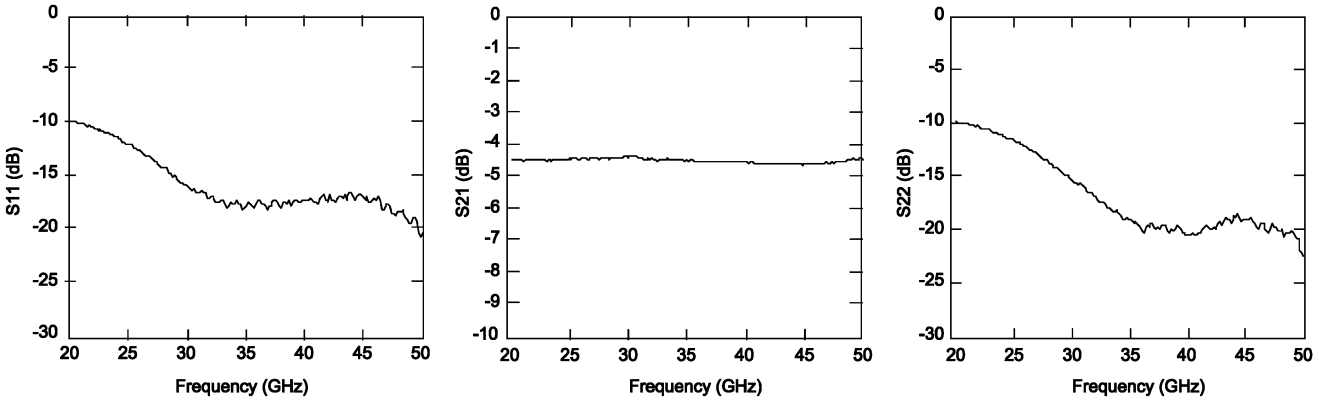

Fig. 15. Measurements of attenuator S-parameters.

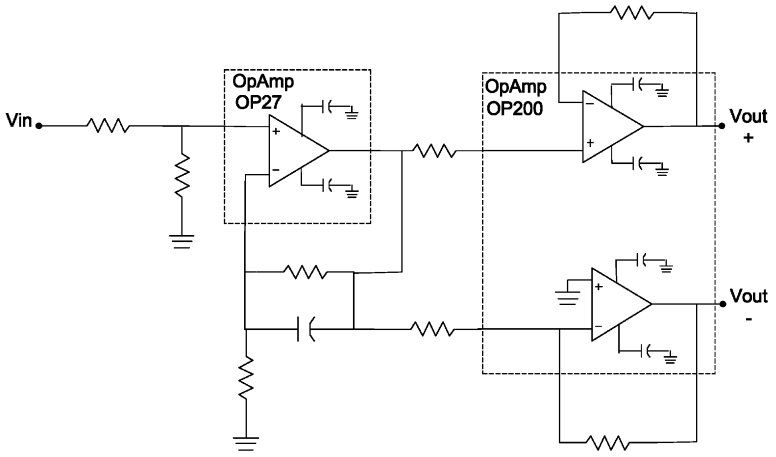

Fig. 16. DC amplifier schematic.

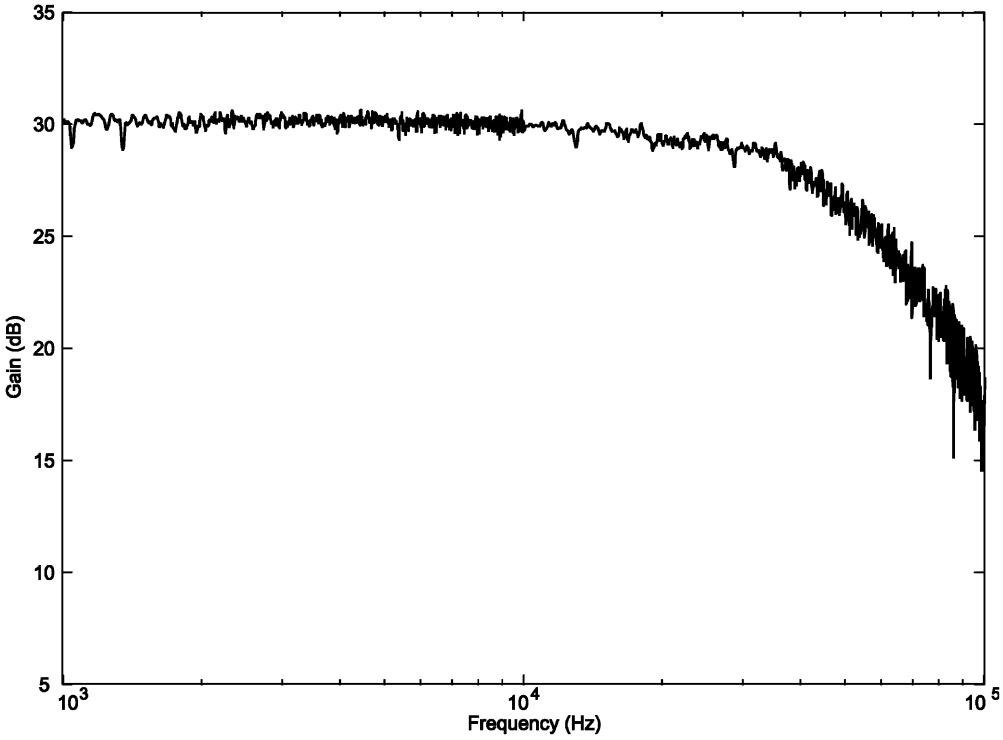

Fig. 17. DC amplifier frequency response.

III. ASSEMBLY

The BEM is a millimeter-wave system, in the mechanical design; assembly and interconnections special attention was paid to some aspects beyond the basic electrical performance, [21]. Each radiofrequency branch was assembled in a carrier where microstrip lines are enclosed in a 2.6 mm wide channel to avoid waveguide mode propagation inside. A cutoff frequency higher than 55 GHz is guaranteed using this enclosure. Fig. 18 shows a detail of microstrip circuits in one branch. From left to right the chain is composed of a 50 Ohm microstrip line, the LNA MMIC N-On, a first microstrip attenuator, the LNA MMIC N-Off, a second microstrip attenuator, bandpass filter and diode detector. All microstrip components and MMIC chips are attached to the metal of the carrier bottom by silver-filled epoxy. Interconnections between microstrip lines and MMICs are made using 25 micron gold wires by ultrasonic bonding. Bias MMIC networks are composed of chip capacitors and thick film resistors to assure amplifier stability at low frequencies. Signal at each branch input comes from a rectangular waveguide connection through the four-section stepped ridge waveguide-to-microstrip line transition.

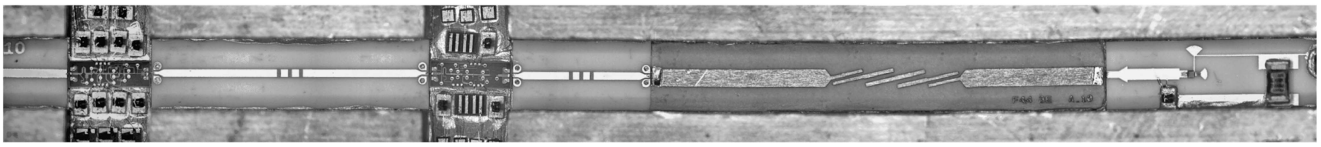

Fig. 18. Detail of RF circuits and diode detector.

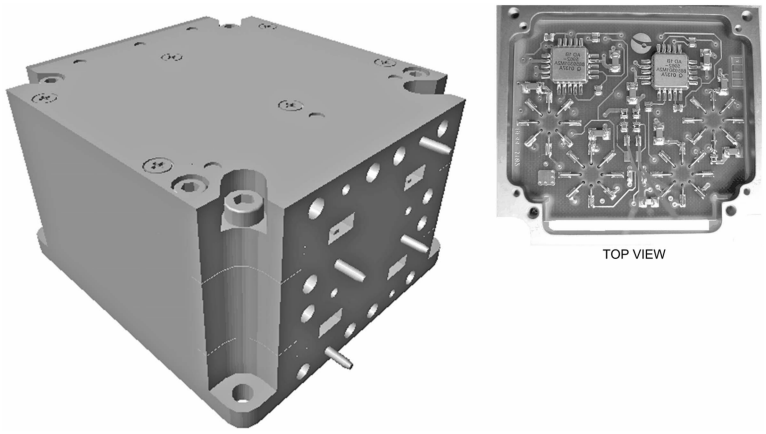

Fig. 19. View of complete BEM with four waveguide inputs and photograph of PCB with dc amplifiers.

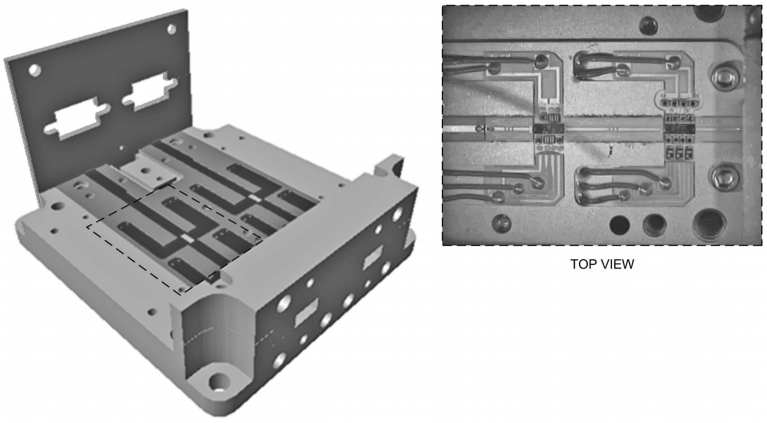

Fig. 20. View of RF carrier with two channels and photograph of one branch with the two MMIC amplifiers.

The final BEM mechanical configuration for the QM has four RF branches, providing signal amplification and detection for two complete radiometers. Mechanical design has been carried out by Mier Comunicaciones S.A. within an assigned envelope of $70 \times 60 \times 39$ mm^3 including all the RF and dc circuitry. Fig. 19 is a frontal view of the complete BEM with four WR-22 waveguide inputs and a top view, when the lid is removed, where there are two dc amplifiers in a printed circuit board (PCB). Multipin miniature connectors at the rear are used for detected signals output and dc polarization lines. The BEM is composed of several layers where multilayer PCBs with dc circuitry and RF carriers are located. Fig. 20 shows an internal view of a BEM's carrier with two RF branches and a photograph showing the lay-out of the MMICs, bias MMIC networks, and microstrip components inside the carrier.

IV. BEM PERFORMANCE

Firstly the RF one-branch BEM performance was tested in order to measure the equivalent temperature of the BEM against frequency. Fig. 21 shows the insertion gain and noise figure measured, where an average RF gain of 35 dB has been obtained. The average noise figure throughout the band was 4.6 dB (560 K). After including the diode detector and dc amplifier in the BEM, several parameters have been measured:

1) dynamic range,
2) sensitivity,
3) RF effective bandwidth,
4) equivalent noise temperature,
5) low frequency power spectrum,
6) output signal video bandwidth.

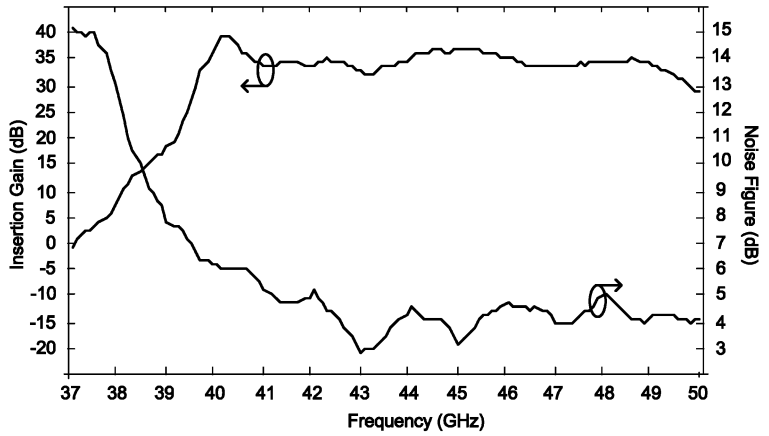

Fig. 21. RF performance of BEM.

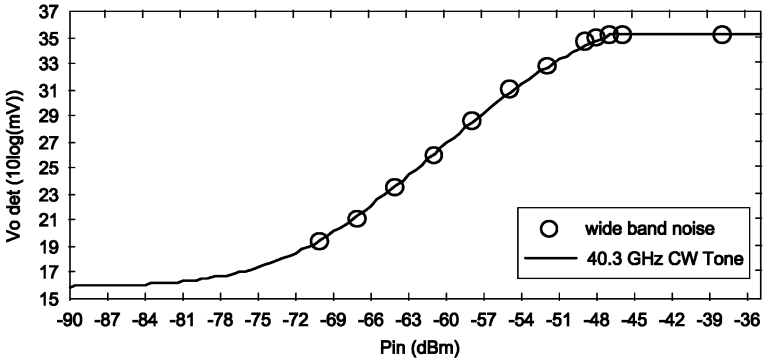

Fig. 22. BEM dynamic range for wideband noise input signal and CW tone.

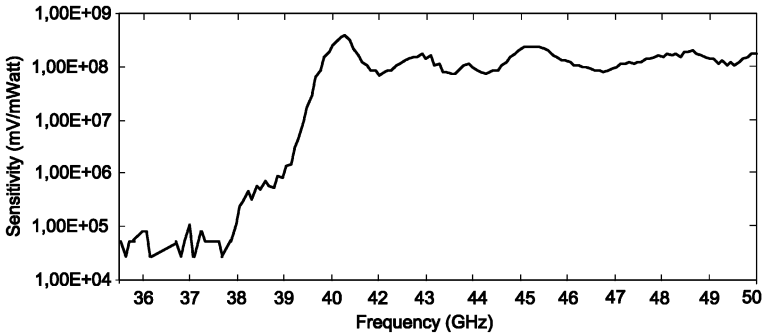

Fig. 23. BEM sensitivity with frequency.

Dynamic Range: The detected voltage versus input power was measured in order to obtain the BEM dynamic range. A HP83650B generator was used as CW source. Results are depicted in Fig. 22 (continuous trace) for 40.3 GHz input frequency. Taking into account the FEM gain, the input power range of the BEM will be between −60 and −56 dBm, depending on whether the radiometer is working in normal operation or in calibration, which corresponds to the linear detection region.

Sensitivity: The BEM performance with frequency was also measured using the HP83650B generator as CW source from 35 to 50 GHz for several input powers. The BEM sensitivity for −56 dBm input power is shown in Fig. 23.

Radiofrequency Effective Bandwidth: In order to use a more realistic input signal, a wideband noise stimulus was used to measure the BEM sensitivity. Fig. 24 shows the set-up used for this test. The results obtained are plotted in Fig. 22 (trace with circles). The measurements shown in Fig. 23 were used in order to calculate the effective bandwidth according to (8). Since the BEM is a direct conversion receiver, the diode detector response must be included in the effective bandwidth expression. This RF to dc response is performed with a microwave

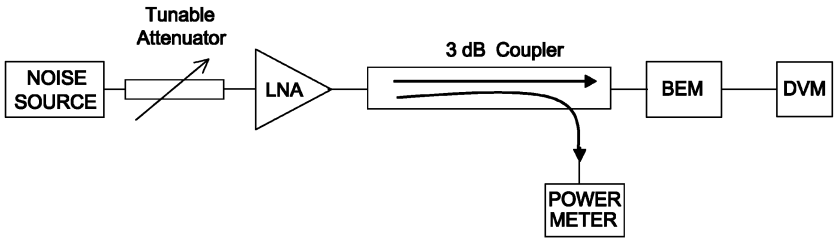

Fig. 24. Wideband noise sensitivity test set-up.

sweep generator providing a constant input power versus frequency, so the effective bandwidth can be calculated using only the output voltage values taken at discrete frequencies as in (10)

$$BW_{\text{eff}} = \Delta f \cdot \left(\frac{N}{N+1}\right) \frac{\left(\sum_{i=1}^{N} V_{\text{out}}(i) - V_{\text{outoff}}\right)^2}{\sum_{i=1}^{N} (V_{\text{out}}(i) - V_{\text{outoff}})^2} \tag{10}$$

where N is the number of frequency points, Δf is the frequency step, $V_{\text{out}}(i)$ is the dc output voltage at each frequency and V_{outoff} is the dc output voltage when the sweep generator is off. The effective bandwidth obtained is 8.9 GHz, slightly wider than the required 20 percent.

Equivalent Noise Temperature: A method has been developed to achieve an accurate and unique equivalent noise temperature of the whole receiver. This method takes into account commercial noise sources, which do not have a flat excess noise ratio versus frequency in millimeter-wave range, and RF to dc receiver performance throughout the band. As the hot temperature of the noise source used and the BEM RF gain show variations across the operating bandwidth, expression (11) was used to obtain the global equivalent temperature (T_{rec}) [22]:

$$T_{\text{rec}} = \frac{\sum_{f1}^{f2} T_h(f) \cdot V_{\text{det}}(f) - Y \cdot T_c \sum_{f1}^{f2} V_{\text{det}}(f)}{(Y-1) \cdot \sum_{f1}^{f2} V_{\text{det}}(f)} \tag{11}$$

where T_h and T_c are the hot and cold temperature of the noise source, Y is the noise Y-factor, and V_{det} is the detected voltage at each frequency when a constant input frequency is applied.

The Y-factor is given by (12), which is based on the ratio of the receiver outputs when looking at two known source temperatures, hot and cold loads.

$$Y = \frac{V_{\text{det}}|_{\text{hot}}}{V_{\text{det}}|_{\text{cold}}}. \tag{12}$$

The Y tested with a cold load and a hot load with commercial noise source Q347B from Agilent was 3.6. Applying (11), the equivalent noise temperature as a total power radiometer was 790 K. This value is slightly worse than the on-wafer measured noise figure of a naked MMIC (3 dB average NF eq. 405 K T_e, see Fig. 6 and Fig. 7). This is due mainly to losses in the waveguide due to microstrip transition and to the readjustment of the bias point to decrease the ripple in the operating band, trading off noise temperature and effective bandwidth. This noise temperature has minimum impact on the global radiometer performance due to the high gain of the FEM.

Low Frequency Power Spectrum: The low frequency power spectrum was characterized with a Hewlett Packard vector signal analyzer HP89410A when a waveguide matched load is connected to the input, and the results are shown in Fig. 25. The test was done at room temperature ($\sim$ 290 K). The $1/f$ knee frequency is around 200 Hz, much lower than the phase switching of the FEM (4096 Hz), so gain fluctuations of the BEM will not have an impact on the global performance of the radiometer. The dominant $1/f$ noise source is attributed to the Schottky diode detector, since it refers directly to the diode current [23]. The $1/f$ noise spectrum of each LNA alone was tested and the knee frequency was about 13 Hz for the N-ON LNA and about 15 Hz for the N-OFF LNA. These results make it evident that the diode detector is mainly responsible for the knee frequency of the BEM.

Output Signal Video Bandwidth: The same test set-up used to test the low frequency spectrum was used to measure the output signal bandwidth. Fig. 26 shows the output spectrum, where a 3 dB bandwidth wider than 50 KHz was obtained. The output signal from the BEM is a square waveform at 4096 Hz, so its main harmonic content can be considered to be below 50 KHz.

V. CONCLUSION

This work reported here is the development of a BEM for space-borne radiometers for the on-going Planck mission of the European Space Agency. A brief description of the Planck LFI radiometer principle of operation has been presented. The design and implementation of a fully representative branch of the 44 GHz BEM for the QM version has been described. Design fundamentals and test performance of each subsystem from RF to dc parts have been presented. An integrated branch has been characterized showing design, assembly, and test procedures to obtain dynamic range, sensitivity, global noise equivalent temperature, $1/f$ knee frequency, and

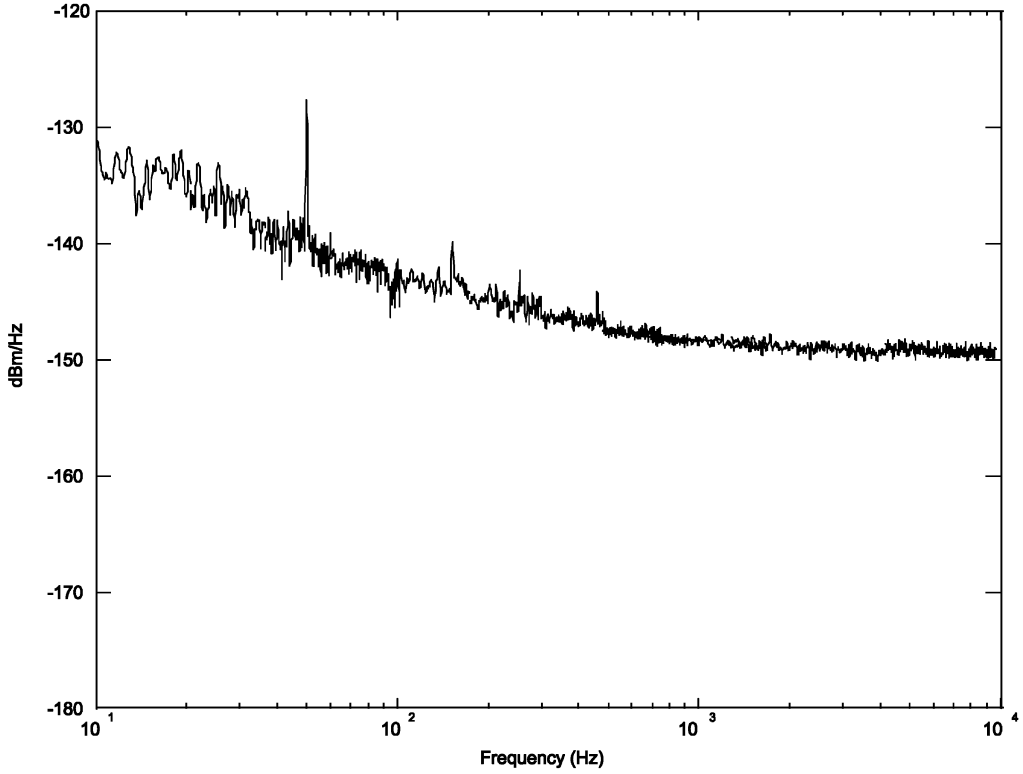

Fig. 25. Low frequency power spectra of output signal.

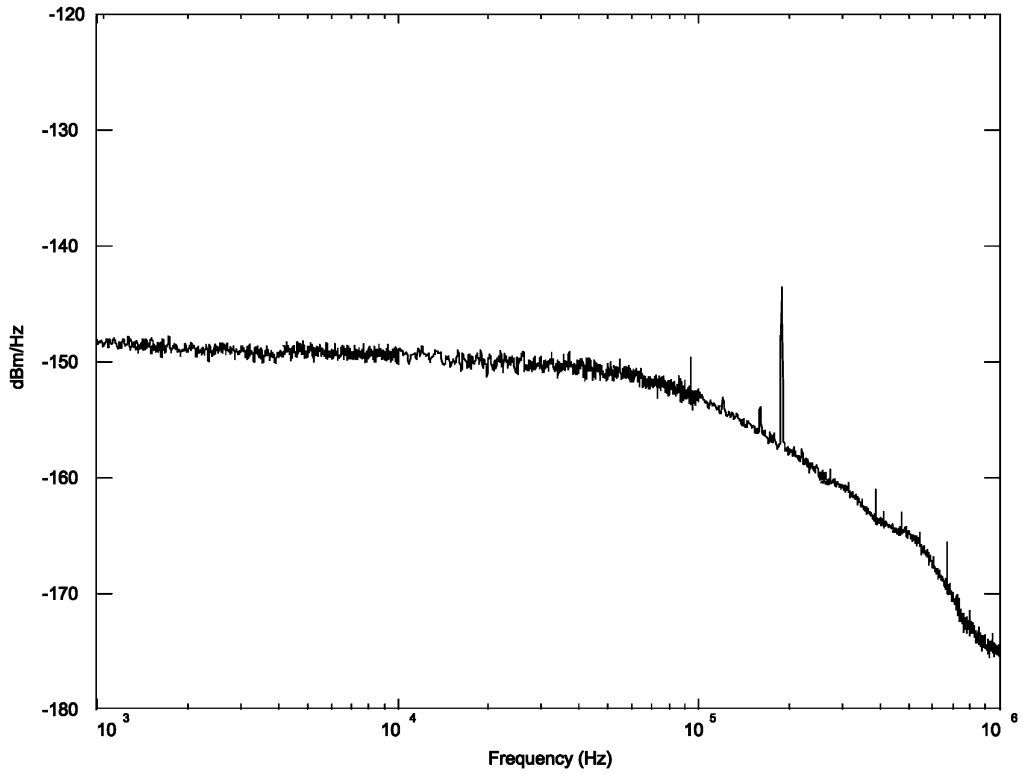

Fig. 26. Output signal bandwidth.

output signal video bandwidth. Some of these figures of merit were measured not only with a single tone, but also with a more realistic input signal, provided with a wideband noise stimulus. The BEM, as a single module, has an adequate performance according to the requirements and the same behavior will be expected after the integration of the FEM and BEM to operate as a complete radiometer.

ACKNOWLEDGMENT

The authors would like to thank Eva Ma Cuerno and Elena Alexandrina Pana for their assistance in the assembly of these circuits and to Mier Comunicaciones S.A. for their help in the mechanical design.

REFERENCES

[1] Bersanelli, M., Mandolesi, N., and Marti-Canales, J.
Multi-band radiometer for measuring the cosmic microwave background.
In *Proceedings of 32nd European Microwave Conference*, Milan, Italy, Sept. 2002, 547–550.

[2] Bersanelli, M., Mandolesi, N., Weinreb, S., Ambrosini, R., and Smoot, G. F.
The LFI differential receiver concept.
Internal report ITESRE 177/1995-COBRAS memo 5, 1995.

[3] Menella, A., et al.
Advanced pseudo-correlation radiometers for the Planck-LFI instrument.
In *Proceedings of the 3rd ESA Workshop on Millimeter Wave Technology and Applications*, Millilab, Espoo, Finland, May 2003, 69–74.

[4] Roddis, N., Kettle, D., Winder, F., Aja, B., Artal, E., de la Fuente, M. L., Pascual, J. P., Mediavilla, A., Pradell, L., and de Paco, P.
Differential radiometer at 30 GHz for the Planck mission.
In *Proceedings of the 3rd ESA Workshop on Millimeter Wave Technology and Techniques and Applications*, Millilab, Espoo, Finland, May 2003, 81–86.

[5] Tuovinen, J., Hughes, N., Jukkala, P., Kangaslahti, P., Karttaavi, T., Sjoman, P., and Varis, J.
Technology for millimetre wave radiometers.
In *Proceedings of the 33rd European Microwave Conference*, Munich, Oct. 2003, 883–886.

[6] Morgante, G., Barber, D., Bhandari, P., Bowman, R. C., Cowgill, P., Crumb, D., Loc, T., Nash, A., Pearson, D., Prina, M., Sirbi, A., Schemlzel, M., Sugimura, R., and Wade, L. A.
Two hydrogen sorption cryocoolers for the Planck mission.
AIP Conference Proceedings, **616**, 1 (May 2002), 298–302.

[7] Seiffert, M., Menella, A., Burigana, C., Mandolesi, N., Bersanelli, M., Meinhold, P., and Lubin, P.
$1/f$ noise and other systematic effects in the Planck-LFI radiometers.
Astronomy & Astrophysics, **391** (2002), 1185–1197.

[8] Tiuri, M. E.
Radio astronomy receivers.
IEEE Transactions on Antennas and Propagation, **AP-12** (Dec. 1964), 930–938.

[9] Mennella, A., Bersanelli, M., Seiffert, M., Kettle, D., Roddis, N., Wilkinson, A., and Meinhold, P.
Offset balancing in pseudo-correlation radiometers for CMB measurements.
Astronomy & Astrophysics, **410** (Nov. 2003), 1089–1100.

[10] Pospieszalski, M. W., Wollack, E. J., Bailey, N., Thacker, D., Webber, J., Nguyen, L. D., and Minh Le, M. L.
Design and performance of wideband, low-noise, millimeter-wave amplifiers for microwave anisotropy probe radiometers.
IEEE Radio Frequency Integrated Circuit Symposium, Digest of Papers, Boston, MA: June 2000, 217–220.

[11] Hoefer, W. J. R., and Burton, M.
Closed-form expressions for the parameters of finned and ridged waveguides.
IEEE Transactions on Microwave Theory and Techniques, **30**, 12 (Dec. 1982), 2190–2194.

[12] Aja, B., de la Fuente, M. L., Pascual, J. P., Mediavilla, A., Cryan, M., and Artal, E.
Q-band monolithic GaAs PHEMT low noise amplifiers: Comparative study of depletion and enhancement mode transistors.
In *Proceedings of the European GAAS 2002 Symposium*, Milan, Italy, Sept. 2002, 53–56.

[13] Engberg, J.
Simultaneous input power match and noise optimisation using feedback.
In *Proceedings of the 4th European Microwave Conference*, 1974, 385–389.

[14] Niclas, K. B.
GaAs MESFET feedback amplifiers: Design considerations and characteristics.
Microwave Journal, (Mar. 1980), 39–48, 85.

[15] Niclas, K. B., Wilser, W. T., Gold, R. B., and Hitchens, W. R.
The matched feedback amplifier: Ultrawide-band microwave amplification with GaAs MESFETs.
IEEE Transactions on Microwave Theory and Techniques, **MTT-28** (Apr. 1980), 285–294.

[16] Lai, R., Chang, K. W., Wang, H., Tan, K., Lo, D. C., Streit, D. C., Liu, P. H., Dia, R., and Berenz, J.
A high performance and low DC power V-band MMIC LNA using 0.1 μm InGaAs/InAlAs/InP HEMT technology.
IEEE Microwave and Guided Wave Letters, **3**, 12 (Dec. 1993), 447–449.

[17] Duh, K. H. G., Liu, S. M. J., Wang, S. C., Ho, P., and Chao, P. C.
High performance Q-band 0.15 μm InGaAs HEMT MMIC LNA.
In *IEEE Microwave and Millimeter-Wave Monolithic Circuits Symposium*, June 1993, 99–102.

[18] Chou, Y. C., Leung, D., Lai, R., Scarpulla, J., Biedenbender, M., Grundbacher, R., Eng, D., Liu, P. H., Oki, A., and Streit, D. C.
High-reliability non-hermetic 0.1 μm GaAs pseudomorphic HEMT MMIC amplifiers.
IEEE Gallium Arsenide Integrated Circ (GaAs IC) Symposium Digest, (2001), 170–173.

[19] Matthaei, G. L., Young, L., and Jones, E. M.
Microwave Filters Impedance-Matching Networks and Coupling Structures.
New York: McGraw-Hill, 1964.

[20] Dettrati, M., Aja, B., Pascual, J. P., de la Fuente, M. L., and Artal, E.
Millimetre wave broadband bandpass microstrip filters. Design and test.
In *Proceedings of the 32nd European Microwave Conference*, Milan, Italy, Sept. 2002, 573–575.

[21] Menzel, W., Kassner, J., and Goebel, U.
Innovative packaging and fabrication concept for a 28 GHz communications front-end.
IEICE, Transactions on Electronics, **E82 C**, 11 (Nov. 1999).

[22] Aja, B., Pascual, J. P., de la Fuente, M. L., Gallegos, J., and Artal, E.
A new method to obtain total power receiver equivalent noise temperature.
In *Proceedings of the 33rd European Microwave Conference*, Munich, Germany, Oct. 2003, 355–358.

[23] Lo, D. C. W., Dow, G. S., Allen, B. R., Yujiri, L., Mussetto, M., Huang, T. W., and Biedendender, M.
A monolithic W-band high-gain LNA/detector for millimetric wave radiometric imaging applications.
Microwave Symposium Digest (1995). (IEEE MTT-S International, vol. 3, May 16–20, 1995, 1117–1120.

Beatriz Aja was born in Santander, Spain. She received the Telecommunications Engineering degree from the University of Cantabria, Santander, Spain, in 1999. She is currently working towards the Ph.D. degree at the same university.

She collaborates in the development of the back end module at 30 GHz, 44 GHz of the differential radiometers in the European Scientific mission Planck. Her areas of interest include the analysis, design and testing of microwave circuits.

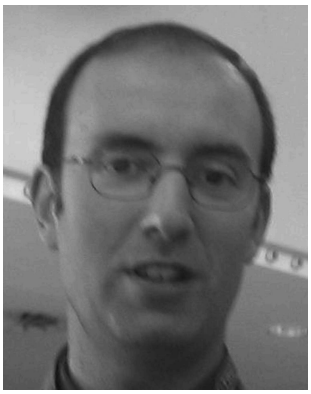

Juan Pablo Pascual was born in Santander, Spain, in 1968. He received the M. degree in electronics with honours in 1990 and the Ph.D. degree in electronic engineering in 1996, both from the University of Cantabria, Santander, Spain.

He is currently an associated professor in the Telecommunications Engineering Department, University of Cantabria. His research interests are HEMT and HBT modelling, MMIC design methodology of linear and nonlinear functions, and system simulation. He has been involved in modelling and design projects with industries from Spain and with international companies and institutions like Daimler Chrysler, Technical University of Darmstadt (where he stayed during 1999) and the Planck scientific mission consortium.

Luisa de la Fuente was born in Reinosa, Spain, in 1968. She graduated from the University of Cantabria, Santander, Spain in 1991 and received the doctoral degree in electronics engineering from the same university in 1997.

From 1992 to 1993, she was an associate teacher in the Department of Electronics, University of Cantabria, where she is currently a professor in the Department of Communication Engineering. Her main research interests include design and testing of microwave circuits in both hybrid and monolithic technologies, in particular, the design of low noise amplifiers and microwave mixers.

Marco Detratti was born in Ravenna, Italy in 1974. He received the Laurea degree (cum laude) in electronic engineering from the University of Perugia, Perugia, Italy, in 2000. He is currently working toward the Ph.D. degree at the University of Cantabria, Santander, Spain.

In 2000, he joined the University of Cantabria to collaborate in the development of the back end module at 44 GHz of the differential radiometers in the European Scientific mission Planck. His research activity involves the design and testing of digital and analogue MMIC for space applications.

Eduardo Artal received the Engineer and Dr. Engineer degrees in telecommunications from the Technical University of Catalonia, Barcelona, Spain, in 1976 and 1982, respectively.

From 1976 to 1990 he was an assistant professor with the Technical University of Catalonia. From 1979 to 1981, on a partial leave from the university, he joined Mier Allende S.A., Barcelona, Spain, where he was involved with TV and FM radio reemitters development. Since 1990 he has been a professor at the University of Cantabria, Santander, Spain, where he was manager of the Telecommunication Engineering course from 1990 to 1994. From 1994 to 1998 he was manager of the National Program for Information and Communications Technologies at the "Plan Nacional de I+D," National R&D Plan in the Spanish Ministry of Education and Science, Madrid. His main areas of activities and contributions have been: microwave circuits and systems, including monolithic microwave integrated circuits from RF (few MHz) up to 50 GHz. His current research interests are low noise millimetre-wave amplifiers and low noise millimetre-wave receivers. He is Project Manager for the back end modules at 30 and 44 GHz for the radiometers of the Planck mission.

Angel Mediavilla was born in Santander, Spain, in 1955. He graduated in 1978 and received the Doctor of Physics (electronic) degree with honors in 1983, both from the University of Cantabria, Santander, Spain.

From 1980 to 1983 he was Ingenieur Stagiere at THOMSON-CSF, France. He is currently professor at the Department of Communications Engineering at the University of Cantabria. He has wide experience in the analysis and optimization of nonlinear microwave active devices in both hybrid and monolithic technologies. He is currently working in the area of nonlinear MESFET/HEMT and HBT device modelling with special application to the large signal computer design and intermodulation properties.

Pedro de Paco was born in Badalona, Spain, in 1972. He received the telecommunication engineering degree and the Ph.D degree from the Technical University of Catalonia (UPC), Barcelona, Spain, in 1997 and 2003, respectively.

In 1998 he joined UPC's Electromagetic and Photonic Engineering Group (EEF) as a graduate student where he was granted a scholarship for the pursuit of his PhD degree. Since June 2004 he has been with Universidad Autonoma de Barcelona, where he teaches courses on microwave circuits and systems. His research interests are in the area of microwave and millimetre-wave circuits and systems design and device modelling.

Lluis Pradell i Cara was born in Barcelona, Catalunya, Spain, in 1956. He received the telecommunication engineering degree from the Universitat Politècnica de Catalunya (UPC), Barcelona, in 1981, and the Dr. degree in telecommunication engineering from UPC in 1989.

From 1981 to 1985 he was with the company Mier-Allende, Barcelona, as an RF & microwave system design engineer. In 1985, he joined the faculty at UPC, where he became associate professor in 1990. Since 1985, he has been teaching courses on microwave circuits, and performing research on models for microwave active devices (MESFET, HEMT, HBT), multimodal models for guiding-structures and transitions (microstrip, finline, slotline, CPW), on-wafer measurement techniques (network-analyzer calibration, noise parameters), development of microwave and millimeter-wave circuits (equipment for space applications, point-to-multipoint broadband equipment, RF MEMS devices), in the frequency range 1 GHz to 75 GHz.